ACS APPLIED MATERIALS & INTERFACES

www.acsami.org

Research Article

Flexible Surface-Enhanced Raman Scattering Chip: A Universal Platform for Real-Time Interfacial Molecular Analysis with Femtomolar Sensitivity

Qi Hao,[▽] Mingze Li,[▽] Jiawei Wang, Xingce Fan, Jie Jiang, Xiaoxia Wang, Minshen Zhu, Teng Qiu,* Libo Ma, Paul K. Chu, and Oliver G. Schmidt

Cite This: *ACS Appl. Mater. Interfaces* 2020, 12, 54174–54180

Read Online

ACCESS | Metrics & More | Article Recommendations | Supporting Information

ABSTRACT: We propose and demonstrate a flexible surface-enhanced Raman scattering (SERS) chip as a versatile platform for femtomolar detection and real-time interfacial molecule analysis. The flexible SERS chip is composed of a flexible and transparent membrane and embedded plasmonic dimers with ultrahigh particle density and ultrasmall dimer gap. The chip enables rapid identification for residuals on solid substrates with irregular surfaces or dissolved analytes in aqueous solution. The sensitivity for liquid-state measurement is down to 0.06 molecule per dimers for 10^{-14} mol·L^{-1} Rhodamine 6G molecule without molecule enrichment. Strong signal fluctuation and blinking are observed at this concentration, indicating that the detection limit is close to the single-molecule level. Meanwhile, the homogeneous liquid environment facilities accurate SERS quantification of analytes with a wide dynamic range. The synergy of flexibility and liquid-state measurement opens up avenues for the real-time study of chemical reactions. The reduction from *p*-nitrothiophenol (PNTP) to *p*-aminothiophenol (PATP) in the absence of the chemical reducing agents is observed at liquid interfaces by in situ SERS measurements, and the plasmon-induced hot electron is demonstrated to drive the catalytic reaction. We believe this robust and feasible approach is promising in extending the SERS technique as a general method for identifying interfacial molecular traces, tracking the evolution of heterogeneous reactions, elucidating the reaction mechanisms, and evaluating the environmental effects such as pH value and salty ions in SERS.

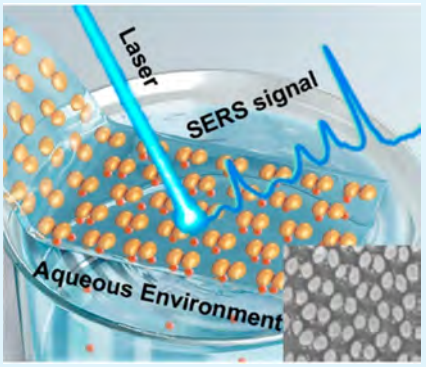

KEYWORDS: *surface-enhanced Raman scattering, plasmonics, dimers, quantitative analysis, liquid state, flexible membrane*

INTRODUCTION

Surface-enhanced Raman scattering (SERS) is a versatile analytical technique featuring ultrahigh sensitivity and specific detection.[1] This technique employs localized surface plasmon resonance (LSPR) to boost the Raman signal of molecules in the vicinity of plasmonic nanostructures.[2] The amplification factor is up to 10^{14}–10^{15}, endowing SERS with the ability of trace molecule detection down to the single-molecule level.[3−7] The immense signal enhancement and the capability in providing molecular vibrational information enable SERS to be a powerful technique to analyze chemical contents of molecules and track their variations during reactions, paving the way for multiple applications in sensing,[8−12] catalysis,[13−16] and environmental monitoring.[17−19]

The performance of SERS is determined by the characteristics of plasmonic materials, which generally refer to noble metallic materials with nanoscale structures.[20] Plasmonic materials can be assembled or fabricated directly on wafers as SERS chips for molecular sensing and analysis. Various fabrication strategies, including electron-beam lithography,[21] focused ion beam,[22,23] colloidal lithography,[24−28] and anodic aluminum oxide (AAO) template methods,[29,30] have been developed to produce and design preferred plasmonic materials to improve SERS efficiency. These strategies have been demonstrated qualified in fabricating homogeneous and reproducible SERS chips with high accuracy, although optimizations in balancing the efficiency and economy are still required. Despite the achievements in nanotechniques, the production of SERS chips depends heavily on the usage of silicon substrates. The annoying high dielectric constants and strong light absorption of the substrates decrease the signal extraction efficiency and limit SERS in the fields of sensing, lasing, and opto-plasmonics where high Q-factors are required.[31−34]

Received: September 10, 2020
Accepted: November 2, 2020
Published: November 18, 2020

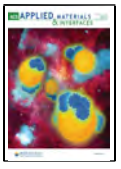

https://dx.doi.org/10.1021/acsami.0c16315
ACS Appl. Mater. Interfaces 2020, 12, 54174–54180

The enhancement factor of SERS is associated with the electromagnetic (EM) fields generated by LSPRs. The intensity of EM fields decreases with the third power of distance, suggesting that efficient SERS only occurs when the molecule is located in the confined region around plasmonic materials.[35] In this case, it is intrinsically difficult to enhance and extract the Raman signal from powder or bulk analytes by placing them on rigid SERS chips. On the other hand, SERS detection with regard to dissolved analytes requires dropping of the solution on SERS chips for molecule adsorption.[36,37] Although this method is qualified in qualitative analysis, a "coffee ring" of previously dissolved analytes is inevitably left behind on the substrates after drying,[38] leading to heterogeneous molecule adsorption. The heterogeneity leads to poor signal reproducibility from region to region and from sample to sample, resulting in an insurmountable obstacle in quantitative SERS. A feasible solution to the heterogeneity is to design a monomolecular layer of the analytes on plasmonic materials by chemical adsorption.[39] However, this approach only applies to molecules with specific chemical bonds, and supplemental chemicals like molecular linkers are generally required.

Herein, we propose and demonstrate a highly active, transparent, and flexible SERS chip to eliminate the limitations of rigid SERS substrates. The flexible chip is composed of a transparent polymer membrane with a functional plasmonic nanoarray bound to its lower surface. Plasmonic dimers, the simplest but most efficient unit structures,[40,41] are closely packed in the nanoarray with a particle density of $10^{10}/cm^2$, providing a giant SERS enhancement with a detection limit down to 10^{-14} mol·L^{-1} for Rhodamine 6G (R6G) solution without molecular enrichment. The good flexibility permits convenient transfer onto target analytes, offering efficient surface coverage for bulk and powder samples while disregarding the surface roughness. Meanwhile, the chip spreads and floats on an aqueous solution, enabling direct SERS detection in the liquid state, where homogeneous molecule adsorption is guaranteed. In addition, real-time analysis of plasmon-induced photocatalysis is performed by studying the reduction from PNTP to PATP with a floating SERS chip, showing the flexibility and efficiency in real time and in situ SERS analysis at liquid interfaces.

The plasmonic dimer arrays are fabricated on silicon substrates by using 200 nm thick ultrathin AAO nanomasks in template-assisted shadow evaporation, as depicted in Figure 1.[42] This method features efficient, reproducible, and large-scale fabrication of plasmonic dimers with sub-10 nm gaps.[43] The details and tricks for fabricating and manipulating the AAO membranes are introduced in the Supporting Information. The AAO membranes with a pore size of 80 nm are fabricated and transferred onto a silicon wafer substrate for shadow deposition (Figure 1b). The two-turn shadow deposition processes are performed by adjusting the deposition angles by calculating the pore-length aspect ratio of AAO. It should be noted that the deposition angle should be recalculated in the second-turn evaporation because the pore diameter and membrane thickness are changed in the first-turn evaporation. The AAO nanomasks are removed from the substrates after evaporation (Figure 1c). The obtained dimers are protected by a poly(methyl methacrylate) (PMMA) polymer membrane by spin-coating (Figure 1d) and subsequently peeled off from the substrate in hot alkali solution (Figure 1e), in this way obtaining the flexible SERS chips. The obtained membrane allows a flexible transfer on target substrates or solution for SERS detection.

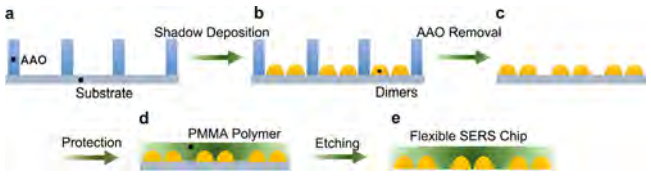

Figure 1. Schematics of the fabrication process. (a) Fabricated ultrathin AAO mask on silicon substrate, (b) fabrication of plasmonic dimer arrays by E-beam shadow deposition, (c) removal of the AAO mask with tape, (d) protection of dimers by spin-coating a PMMA protection layer on top, and (e) removal of the silicon substrate in alkaline solution.

The SERS chip is demonstrated in identifying and analyzing the component of colorants on the rough surface by a proof-of-concept study. Figure 2a shows the fabricated SERS chip with dimer patterns floating on water. The dimer gap is estimated to be 8−12 nm in average, indicating dense "hot spots" between two dimer particles. The chip is transferred onto rough polyvinyl chloride paper to identify the dyes in oil-based pen inks (STABILO, Permanent). As illustrated in Figure 2b, a small letter "a" is written on the paper and subsequently washed away by acetone. The chip is transferred onto the area of interest where "a" was written to detect the residual molecules. The van der Waals force between the chip and the substrate provides good adhesion, which allows close contact between the dimers and the target molecules even on irregular surfaces with microscale roughness (Figure S2). Figure 2e compares the Raman spectra from the area of interest with ink and the blank area without ink under 458 nm laser irradiation. The characteristic bands of Victoria Blue B and Rhodamine B are discerned from the ink, but Victoria Blue B can be hardly

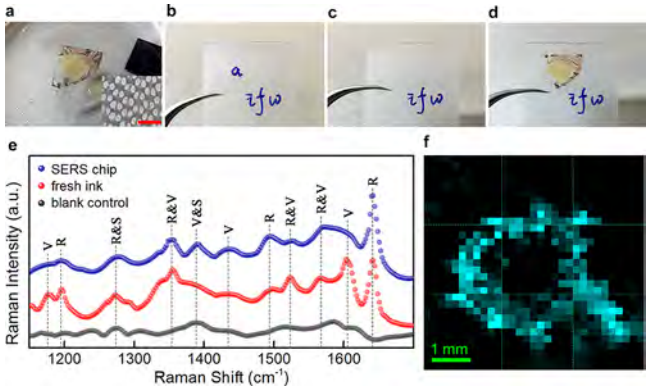

Figure 2. Flexible SERS chips in in situ identification and characterization of colorants. (a) Optical photo of the fabricated flexible SERS chip on water. The inset shows a scanning electron microscopy image of the plasmonic dimer array with the scale bar being 200 nm. (b−d) Optical photos illustrating the experimental process: a small letter "a" is written on rough polyvinyl chloride paper (b) and subsequently washed away by acetone (c). Afterward, the SERS chip is transferred onto the area of interest for SERS detection (d). (e) Raman spectra from the area of interest, fresh ink, and blank control. The Raman peaks of Rhodamine B (R), Victoria blue B (V), and substrate (S) are marked. (f) SERS maps from the area of interest by analyzing the integrated intensity at 1642 cm^{-1}. The maps are composed of 9 pieces of a 2D Raman map by measuring 121 points in each map with a scanning step of 200 μm.

https://dx.doi.org/10.1021/acsami.0c16315
ACS Appl. Mater. Interfaces 2020, 12, 54174−54180

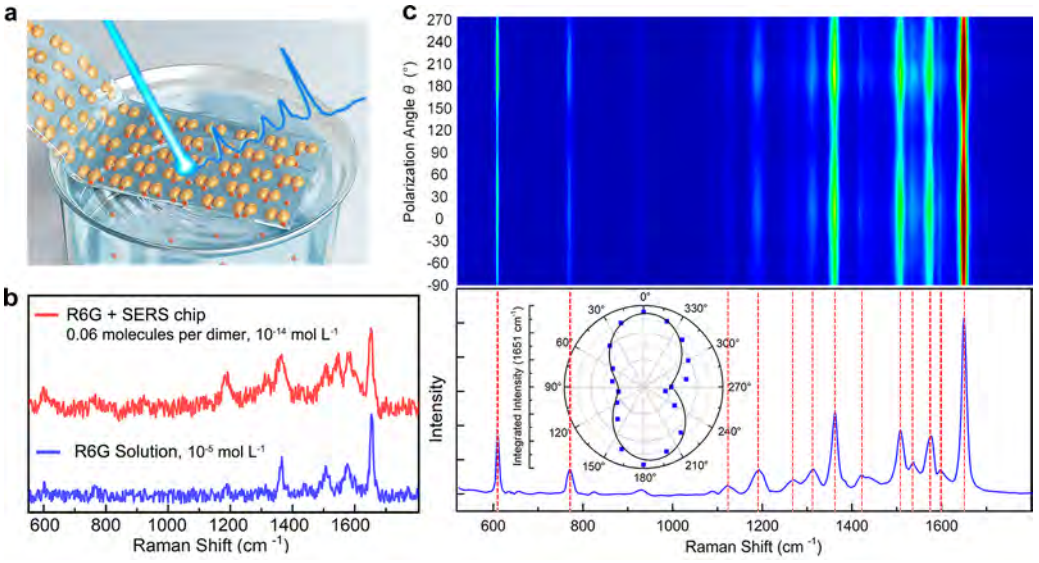

Figure 3. Performance of the flexible SERS chips. (a) Schematic of liquid-state SERS measurement using the flexible SERS chip. (b) Typical Raman spectra of R6G with and without the chip. The SERS spectrum taken at 10^{-14} mol·L^{-1} exhibits strong signal fluctuation and blinking, indicating that the molecular concentration is close to the single-molecule level. (c) Raman map of R6G as a function of polarization angle θ and the Raman spectrum taken with the laser polarization being parallel (θ = 0°) to the dimer long axis. The inset depicts the integrated Raman intensity at 1651 cm^{-1} as a function of θ.

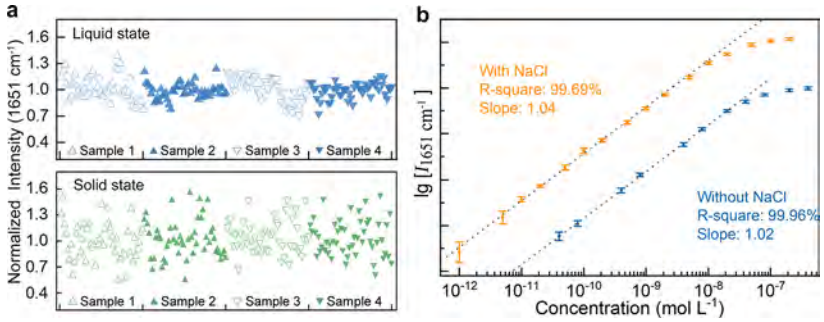

Figure 4. (a) Integrated Raman intensity at 1651 cm^{-1} at random measurement sites over a large scale in liquid-state and solid-state SERS measurements, respectively. The samples are fabricated under the same experimental conditions. (b) Logarithm of the integrated Raman intensity at 1651 cm^{-1} as a function of molecular concentration and corresponding fitting curves in liquid-state SERS.

found in the area of interest, suggesting that only Rhodamine B is preserved. It is known that Rhodamine B adsorbs to plastic materials so the ink color could be permanent. The photoluminescence spectrum of Rhodamine B is located in the yellow and red wavelength region, and the presence of Victoria Blue B helps to correct this chromatic aberration. Figure 2f exhibits the point-by-point Raman maps of the 1642 cm^{-1} band from the area of interest where the profile of the letter "a" is clearly revealed, suggesting the potential of flexible SERS chips in identifying text contents of ancient calligraphy and painting for archeological applications.

Figure 3a shows a schematic of the flexible SERS chip in liquid-state Raman measurements. The SERS efficiency of the dimer chip is illustrated by comparing the Raman spectra on R6G aqueous solution with and without the SERS chip (Figure 3b). The dimer chip exhibits a discernible detection concentration as low as 10^{-14} mol·L^{-1} in 20 mL of R6G solution by optimizing the laser polarization. The molecular areal density is calculated to be <0.06 molecule per dimer in a limiting case assuming that all of the molecules are adsorbed on the chip. It is notable that SERS spectra taken at 10^{-14} mol·L^{-1} exhibit strong signal fluctuation. In most cases, the SERS signal is not available. This might arise from the random adsorption of molecules, which leads to a Poisson distribution in the SERS measurement. The signal drifting or blinking is also observed during the measurement, suggesting that the detection is close to the single-molecule level. The Raman map of R6G as a function of polarization angle θ in depicted in Figure 3c. The result suggests that the maximum enhancement only occurs when the laser polarization is parallel to the dimer long axis, revealing the efficiency of the patterned dimer arrays.

Figure 4a evaluates the signal homogeneity and reproducibility in liquid-state and solid-state SERS by measuring the Raman spectra from dimer samples fabricated under the same experimental conditions (also see Figure S3). The samples for solid-state measurement are immersed in R6G solution for 10 h to establish the adsorption equilibrium and quickly dried with nitrogen gas. In liquid-state SERS, the samples float on R6G solution all the time for adsorption and measurements. The results in Figure 4a reveal that there is a clear improvement in signal homogeneity with liquid-state measurement, suggesting that the dying process in solid-state measurement results in inevitable heterogeneity. The reproducibility is the bottleneck in solid-state SERS in quantitative

https://dx.doi.org/10.1021/acsami.0c16315
ACS Appl. Mater. Interfaces 2020, 12, 54174−54180

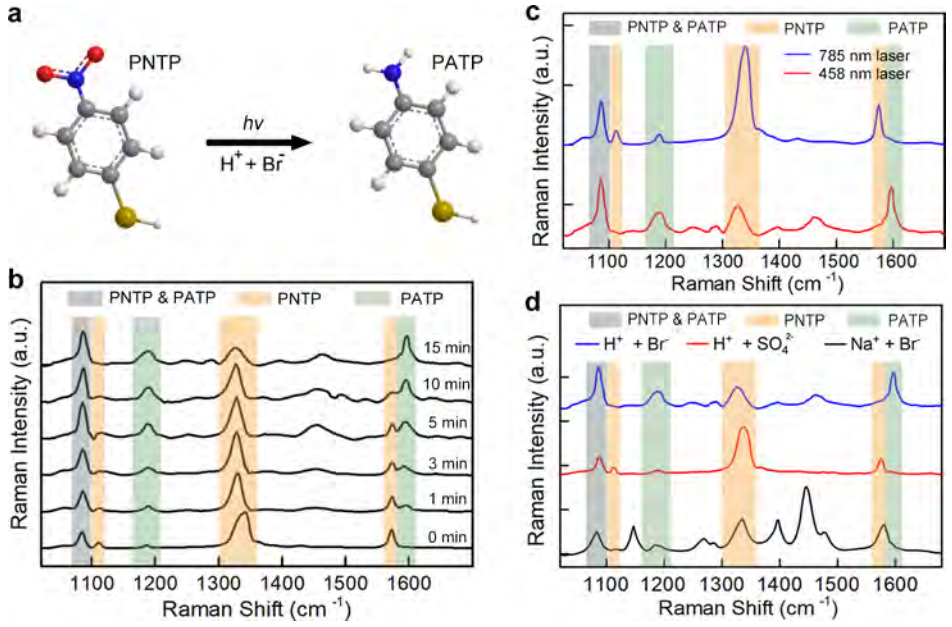

Figure 5. (a) Schematic and (b) SERS dynamics of the reduction from *p*-nitrothiophenol (PNTP) to *p*-aminothiophenol (PATP) under irradiation. (c) SERS spectra of the analytes after 15 min of irradiation under 458 and 785 nm laser. (d) Effects of ions on the reduction from PNTP to PATP.

analysis. It arises from the irregular distribution of the hot spots and the heterogeneity in molecular areal density. The heterogeneity is obvious when the measurement sites are picked over a microscopic distance (>10 μm) or from different samples, while homogeneity is observed when the sites are located within a limited area (Figure S4).

Figure 4b shows the working curves of the Raman intensity with R6G concentration in the logarithmic scale. The results exhibit a well-defined linear response to the molecular concentration in an unprecedented wide dynamic range, which is probably due to the homogeneous liquid environment and the ultrahigh particle density of $10^{10}/cm^2$. The linear response region in SERS analysis is generally limited to specific working concentrations because the surface adsorption gets saturated at high concentrations while random adsorption of molecules results in a strong signal fluctuation at the low end. When chloride ions are added, the working region is extended from 5×10^{-10} to 1×10^{-12} mol·L^{-1} due to extra 2 orders of magnitude enhancement from the chloride activation. Previous research considered that it may arise from particle aggregations or ion-induced surface roughness.[44−46] Figure 4b reveals that the addition of chloride ions has modified the quantitative linear range at high concentration, suggesting that the adsorption equilibrium has been reestablished. This indicates that there should be other mechanisms responsible for the chloride activation.

Figure 5 represents the real-time in situ observation of Raman spectra in plasmon-induced photocatalytic reduction by using flexible SERS chips in liquid-state measurements. The dynamics of the reduction from *p*-nitrothiophenol (PNTP) to *p*-aminothiophenol (PATP) on the silver surface are observed under 458 nm resonance laser irradiation as shown Figure 5b. The chips are placed on 10^{-6} mol·L^{-1} PNTP solution for molecular adsorption and then transferred to the hydrobromic acid solution for laser irradiation and reaction. The SERS spectrum before irradiation exhibits the characteristic bands of PNTP at 1083, 1112, 1338, and 1567 cm^{-1}, which are attributed to the C−N stretching, C−S stretching, $-NO_2$ symmetric stretching, and parallel C−C stretching modes, respectively. When exposed to resonance laser irradiation at 458 nm, new vibrational Raman bands at 1176 and 1590 cm^{-1} corresponding to PATP molecules appear and are assigned to the C−H bending and C−C stretching, respectively. We also observe a shift of the 1338 cm^{-1} mode and an unmarked new mode at 1455 cm^{-1}, which may arise from PATP or other surface species generated by reversible reactions.[47]

It should be noted that the reduction from PNTP to PATP does not occur on the silver surface in the absence of chemical reducing agents due to the charge-carrier recombination in silver. When bromine ions are added, silver bromide forms at the silver surface and they dissociate under irradiation.[48] This redox reaction establishes the recycling of Ag atoms and provides continuous hot electrons to the reactants. With the assistance of the hot electrons and hydrogen ions, the PNTP molecules are gradually reduced to PATP. Figure 5c reveals that this reduction occurs only when the irradiation wavelength is in resonance with the plasmon resonance profile, indicating that the hot electrons generated by LSPR are responsible for the reduction. To evaluate the effects of ions, the reduction is studied in the presence of hydrogen and bromine ions, respectively, as shown in Figure 5d. The characteristic peaks of PATP are observed when hydrogen and bromide ions work simultaneously, while peaks of PNTP or *p*,*p*′-dimercaptoazobenzene (DMAB) molecules are observed in the presence of only hydrogen ions or only bromic ions, respectively. The peaks of DMAB can be observed under neutral or alkaline environments, and detailed discussions are available in Figure S5. The reduction from PNTP to PATP is also applicable to other halogen ions (Figure S6).

CONCLUSION

This article depicts the versatility of flexible SERS chips in scientific research and practical applications. The chip features an ultrahigh particle density and ultrasmall gaps between

https://dx.doi.org/10.1021/acsami.0c16315
ACS Appl. Mater. Interfaces 2020, 12, 54174−54180

dimers, providing outstanding sensitivity on the single-molecule level and homogeneous hot spots for quantitative analysis. The flexible chip is demonstrated to be promising in nondestructive identification of text information and pigment compositions for archeological applications, as well as a qualified candidate in liquid-state SERS with excellent sensitivity down to 0.06 molecule per dimers for 10^{-14} mol·L^{-1} R6G molecule without molecule enrichment. It also enables real-time in situ SERS measurements in a liquid environment, where an ideal homogeneous environment is guaranteed. We observed the reduction from PNTP to PATP in the absence of chemical reducing agents by in situ liquid-state Raman measurement and demonstrated that plasmon-induced hot electrons drive this catalytic reaction. This easy-to-use and low-cost SERS chip offers a functional platform to study heterogeneous catalysis, elucidate the reaction mechanisms, and evaluate the ion effects. We believe the versatility and flexibility will enable SERS as a standard characterization method in general scientific communities.

EXPERIMENTAL SECTION

Fabrication of Patterned Nanoarrays Using Ultrathin Anodic Aluminum Oxide Membranes. The plasmonic particle/dimer arrays were fabricated on silicon or quartz substrates by using anodic aluminum oxide (AAO) membranes in shadow evaporation.[42] The details about how to fabricate and manipulate ultrathin AAO membranes are available in the Supporting Information. The film thickness and pore size of the AAO membranes were 200 and 80 nm, respectively. The silver dimers are fabricated by performing a two-step angle-resolved shadow deposition with an opposite deposition angle in each turn. The particle size and dimer gap were controlled by adjusting the AAO pore size and evaporation angles in E-beam deposition, in this way optimizing the plasmon resonance mode of dimers to couple with the 458 nm irradiation laser.

Fabrication of the Flexible SERS Chips. Highly transparent PMMA membranes were spin-coated onto the prepared nanoarrays and then baked at 120 °C for 5 min. The membranes were peeled off with the intact nanoarrays in 1 M hot alkali solution at 90 °C for 15 min and then transferred to distilled water. The PMMA membranes exhibit 99% transparency in the visible range (Figure S7).

Raman Measurement. R6G and PNTP molecules were purchased from Sigma-Aldrich. During the preparation procedures, all the cuvettes were immersed with a portion of the sample solutions and rinsed several times to establish an equilibrium between adsorption and dissolution. The pipettes were flushed several times to reduce wall adsorption. The cuvettes were placed on an antishock rubber pad for SERS measurement. The chips were glued at the cuvette edge by a droplet of water to decrease the effects of solution fluctuations. A 458 nm laser was used as the irradiation and excitation source for all experiments. The laser spot in quantitative measurement was enlarged from 1 to 10 μm for better signal uniformity.[49,50] In plasmon-induced photocatalysis, the chips were placed on 10^{-6} mol·L^{-1} PNTP solution for 24 h and then transferred to 0.1 M hydrobromic solution for irradiation and measurement. The laser powers for irradiation and Raman measurement were set at 0.1 and 0.01 mW, respectively.

ASSOCIATED CONTENT

Supporting Information

The Supporting Information is available free of charge at https://pubs.acs.org/doi/10.1021/acsami.0c16315.

Method of fabricating plasmonic nanoarrays using ultrathin anodic aluminum oxide (AAO) membranes; proof-of-concept experiment demonstrating the good adhesion between the flexible SERS chip and the substrates; relative standard deviation (RSD) of Raman signals in liquid-state SERS measurements; dispersion of Raman intensity in solid-state measurement; and additional analysis data about the real-time in situ observation of Raman spectra in plasmon-induced photocatalytic reduction (PDF)

AUTHOR INFORMATION

Corresponding Author

Teng Qiu − *School of Physics, Southeast University, Nanjing 211189, P. R. China;* orcid.org/0000-0002-1160-2619; Email: tqiu@seu.edu.cn

Authors

Qi Hao − *School of Physics and Quantum Information Research Center, Southeast University, Nanjing 211189, P. R. China; Institute for Integrative Nanosciences, Leibniz IFW Dresden, Dresden 01069, Germany;* orcid.org/0000-0002-5525-4417

Mingze Li − *School of Physics, Southeast University, Nanjing 211189, P. R. China;* orcid.org/0000-0001-8271-5576

Jiawei Wang − *Institute for Integrative Nanosciences, Leibniz IFW Dresden, Dresden 01069, Germany; Department of Electronic and Information Engineering, Harbin Institute of Technology (Shenzhen), Shenzhen 518055, P. R. China;* orcid.org/0000-0001-6323-8081

Xingce Fan − *School of Physics, Southeast University, Nanjing 211189, P. R. China; Institute for Integrative Nanosciences, Leibniz IFW Dresden, Dresden 01069, Germany;* orcid.org/0000-0002-2508-3063

Jie Jiang − *School of Physics, Southeast University, Nanjing 211189, P. R. China*

Xiaoxia Wang − *Institute for Integrative Nanosciences, Leibniz IFW Dresden, Dresden 01069, Germany*

Minshen Zhu − *Institute for Integrative Nanosciences, Leibniz IFW Dresden, Dresden 01069, Germany;* orcid.org/0000-0001-5883-4962

Libo Ma − *Institute for Integrative Nanosciences, Leibniz IFW Dresden, Dresden 01069, Germany;* orcid.org/0000-0001-9850-2292

Paul K. Chu − *Department of Physics, Department of Materials Science and Engineering, and Department of Biomedical Engineering, City University of Hong Kong, Hong Kong 999077, P. R. China;* orcid.org/0000-0002-5581-4883

Oliver G. Schmidt − *Institute for Integrative Nanosciences, Leibniz IFW Dresden, Dresden 01069, Germany; Material Systems for Nanoelectronics, Technische Universität Chemnitz, Chemnitz 09111, Germany*

Complete contact information is available at: https://pubs.acs.org/10.1021/acsami.0c16315

Author Contributions

$^{\nabla}$Q.H. and M.L. contributed equally.

Notes

The authors declare no competing financial interest.

ACKNOWLEDGMENTS

The authors thank R. Engelhard and S. Baunack for technical support. Q.H. acknowledges the National Natural Science Foundation of China (Grant no. 22004016) and the Fundamental Research Funds for the Central Universities. T.Q. acknowledges the National Key R&D Program of China

(Grant no. 2017YFA0403600) and the National Natural Science Foundation of China (Grant No. 11874108)O.G.S. acknowledges the German Research Foundation DFG (Grant FOR 1713).

REFERENCES

(1) Stiles, P. L.; Dieringer, J. A.; Shah, N. C.; Van Duyne, R. P. Surface-Enhanced Raman Spectroscopy. *Annu. Rev. Anal. Chem.* **2008**, *1*, 601−626.
(2) Ding, S. Y.; You, E. M.; Tian, Z. Q.; Moskovits, M. Electromagnetic Theories of Surface-Enhanced Raman Spectroscopy. *Chem. Soc. Rev.* **2017**, *46* (13), 4042−4076.
(3) Nie, S.; Emory, S. R. Probing Single Molecules and Single Nanoparticles by Surface-Enhanced Raman Scattering. *Science* **1997**, *275* (5303), 1102−1106.
(4) Camden, J. P.; Dieringer, J. A.; Wang, Y.; Masiello, D. J.; Marks, L. D.; Schatz, G. C.; Van Duyne, R. P. Probing the Structure of Single-Molecule Surface-Enhanced Raman Scattering Hot Spots. *J. Am. Chem. Soc.* **2008**, *130* (38), 12616−12617.
(5) Lim, D. K.; Jeon, K. S.; Kim, H. M.; Nam, J. M.; Suh, Y. D. Nanogap-Engineerable Raman-Active Nanodumbbells for Single-Molecule Detection. *Nat. Mater.* **2010**, *9* (1), 60−67.
(6) Lim, D. K.; Jeon, K. S.; Hwang, J. H.; Kim, H.; Kwon, S.; Suh, Y. D.; Nam, J. M. Highly Uniform and Reproducible Surface-Enhanced Raman Scattering from DNA-Tailorable Nanoparticles with 1-Nm Interior Gap. *Nat. Nanotechnol.* **2011**, *6* (7), 452−460.
(7) Yang, S.; Dai, X.; Stogin, B. B.; Wong, T. S. Ultrasensitive Surface-Enhanced Raman Scattering Detection in Common Fluids. *Proc. Natl. Acad. Sci. U. S. A.* **2016**, *113* (2), 268−273.
(8) Anker, J. N.; Hall, W. P.; Lyandres, O.; Shah, N. C.; Zhao, J.; Van Duyne, R. P. Biosensing with Plasmonic Nanosensors. *Nanosci. Technol.* **2009**, 308−319.
(9) Qian, X.; Li, J.; Nie, S. Stimuli-Responsive SERS Nanoparticles: Conformational Control of Plasmonic Coupling and Surface Raman Enhancement. *J. Am. Chem. Soc.* **2009**, *131* (22), 7540−7541.
(10) Liu, N.; Tang, M. L.; Hentschel, M.; Giessen, H.; Alivisatos, A. P. Nanoantenna-Enhanced Gas Sensing in a Single Tailored Nanofocus. *Nat. Mater.* **2011**, *10* (8), 631−636.
(11) Wang, Y.; Zhou, C.; Wang, W.; Xu, D.; Zeng, F.; Zhan, C.; Gu, J.; Li, M.; Zhao, W.; Zhang, J.; et al. Photocatalytically Powered Matchlike Nanomotor for Light-Guided Active SERS Sensing. *Angew. Chem., Int. Ed.* **2018**, *57* (40), 13110−13113.
(12) Guo, J.; Zeng, F.; Guo, J.; Ma, X. Preparation and Application of Microfluidic SERS Substrate: Challenges and Future Perspectives. *J. Mater. Sci. Technol.* **2020**, *37*, 96−103.
(13) van Schrojenstein Lantman, E. M.; Deckert-Gaudig, T.; Mank, A. J.; Deckert, V.; Weckhuysen, B. M. Catalytic Processes Monitored at the Nanoscale with Tip-Enhanced Raman Spectroscopy. *Nat. Nanotechnol.* **2012**, *7* (9), 583−586.
(14) Xie, W.; Walkenfort, B.; Schlücker, S. Label-Free SERS Monitoring of Chemical Reactions Catalyzed by Small Gold Nanoparticles Using 3D Plasmonic Superstructures. *J. Am. Chem. Soc.* **2013**, *135* (5), 1657−1660.
(15) Zhang, H.; Wang, C.; Sun, H. L.; Fu, G.; Chen, S.; Zhang, Y. J.; Chen, B. H.; Anema, J. R.; Yang, Z. L.; Li, J. F.; et al. In Situ Dynamic Tracking of Heterogeneous Nanocatalytic Processes by Shell-Isolated Nanoparticle-Enhanced Raman Spectroscopy. *Nat. Commun.* **2017**, *8*, 15447.
(16) Cortés, E.; Xie, W.; Cambiasso, J.; Jermyn, A. S.; Sundararaman, R.; Narang, P.; Schlücker, S.; Maier, S. A. Plasmonic Hot Electron Transport Drives Nano-Localized Chemistry. *Nat. Commun.* **2017**, *8* (1), 14880.
(17) Vo-Dinh, T. SERS Chemical Sensors and Biosensors: New Tools for Environmental and Biological Analysis. *Sens. Actuators, B* **1995**, *29* (1−3), 183−189.
(18) Wei, H.; Hossein Abtahi, S. M.; Vikesland, P. J. Plasmonic Colorimetric and SERS Sensors for Environmental Analysis. *Environ. Sci.: Nano* **2015**, *2* (2), 120−135.
(19) Zeng, F.; Duan, W.; Zhu, B.; Mu, T.; Zhu, L.; Guo, J.; Ma, X. Paper-Based Versatile Surface-Enhanced Raman Spectroscopy Chip with Smartphone-Based Raman Analyzer for Point-of-Care Application. *Anal. Chem.* **2019**, *91* (1), 1064−1070.
(20) Kelly, K. L.; Coronado, E.; Zhao, L. L.; Schatz, G. C. The Optical Properties of Metal Nanoparticles: The Influence of Size, Shape, and Dielectric Environment. *J. Phys. Chem. B* **2003**, *107* (3), 668−677.
(21) Zhang, W.-Y.; Xiao, X.-Z.; Lv, C.; Zhao, J.; Wang, G.; Gu, X.; Zhang, R.; Xu, B.-B.; Zhang, D.-D.; Li, A.-W.; et al. Fabrication of Photopolymer Hierarchical Micronanostructures by Coupling Electrospinning and Photolithography for SERS Substrates. *Macromol. Res.* **2013**, *21* (3), 306−310.
(22) D'Andrea, C.; Fazio, B.; Gucciardi, P. G.; Giordano, M. C.; Martella, C.; Chiappe, D.; Toma, A.; Buatier de Mongeot, F.; Tantussi, F.; Vasanthakumar, P.; et al. SERS Enhancement and Field Confinement in Nanosensors Based on Self-Organized Gold Nanowires Produced by Ion-Beam Sputtering. *J. Phys. Chem. C* **2014**, *118* (16), 8571−8580.
(23) Sivashanmugan, K.; Liao, J.-D.; You, J.-W.; Wu, C.-L. Focused-Ion-Beam-Fabricated Au/Ag Multilayered Nanorod Array as SERS-Active Substrate for Virus Strain Detection. *Sens. Actuators, B* **2013**, *181*, 361−367.
(24) Grzelczak, M.; Pérez-Juste, J.; Mulvaney, P.; Liz-Marzán, L. M. Shape Control in Gold Nanoparticle Synthesis. *Chem. Soc. Rev.* **2008**, *37* (9), 1783−1791.
(25) Edel, J. B.; Kornyshev, A. A.; Kucernak, A. R.; Urbakh, M. Fundamentals and Applications of Self-Assembled Plasmonic Nanoparticles at Interfaces. *Chem. Soc. Rev.* **2016**, *45* (6), 1581−1596.
(26) Udayabhaskararao, T.; Altantzis, T.; Houben, L.; Coronado-Puchau, M.; Langer, J.; Popovitz-Biro, R.; Liz-Marzán, L. M.; Vuković, L.; Král, P.; Bals, S.; et al. Tunable Porous Nanoallotropes Prepared by Post-Assembly Etching of Binary Nanoparticle Superlattices. *Science* **2017**, *358* (6362), 514−518.
(27) Zhang, T.; Sun, Y.; Hang, L.; Li, H.; Liu, G.; Zhang, X.; Lyu, X.; Cai, W.; Li, Y. Periodic Porous Alloyed Au−Ag Nanosphere Arrays and Their Highly Sensitive SERS Performance with Good Reproducibility and High Density of Hotspots. *ACS Appl. Mater. Interfaces* **2018**, *10* (11), 9792−9801.
(28) Liu, D.; Cai, W.; Marin, M.; Yin, Y.; Li, Y. Air-Liquid Interfacial Self-Assembly of Two-Dimensional Periodic Nanostructured Arrays. *ChemNanoMater.* **2019**, *5* (11), 1338−1360.
(29) Hou, X.; Luo, X.; Fan, X.; Peng, Z.; Qiu, T. Plasmon-Coupled Charge Transfer in WO_{3-x} Semiconductor Nanoarrays: Toward Highly Uniform Silver-Comparable SERS Platforms. *Phys. Chem. Chem. Phys.* **2019**, *21* (5), 2611−2618.
(30) Fan, X.; Hao, Q.; Jin, R.; Huang, H.; Luo, Z.; Yang, X.; Chen, Y.; Han, X.; Sun, M.; Jing, Q.; et al. Assembly of Gold Nanoparticles into Aluminum Nanobowl Array. *Sci. Rep.* **2017**, *7* (1), 2322.
(31) Panneerselvam, R.; Liu, G. K.; Wang, Y. H.; Liu, J. Y.; Ding, S. Y.; Li, J. F.; Wu, D. Y.; Tian, Z. Q. Surface-Enhanced Raman Spectroscopy: Bottlenecks and Future Directions. *Chem. Commun.* **2018**, *54* (1), 10−25.
(32) Zong, C.; Xu, M.; Xu, L. J.; Wei, T.; Ma, X.; Zheng, X. S.; Hu, R.; Ren, B. Surface-Enhanced Raman Spectroscopy for Bioanalysis: Reliability and Challenges. *Chem. Rev.* **2018**, *118* (10), 4946−4980.
(33) Ward, J.; Benson, O. WGM Microresonators: Sensing, Lasing and Fundamental Optics with Microspheres. *Laser Photonics Rev.* **2011**, *5* (4), 553−570.
(34) Chiasera, A.; Dumeige, Y.; Feron, P.; Ferrari, M.; Jestin, Y.; Nunzi Conti, G.; Pelli, S.; Soria, S.; Righini, G. C. Spherical Whispering-Gallery-Mode Microresonators. *Laser Photonics Rev.* **2010**, *4* (3), 457−482.
(35) Otto, A.; Mrozek, I.; Grabhorn, H.; Akemann, W. Surface-Enhanced Raman Scattering. *J. Phys.: Condens. Matter* **1992**, *4* (5), 1143.
(36) Li, P.; Li, Y.; Zhou, Z. K.; Tang, S.; Yu, X. F.; Xiao, S.; Wu, Z.; Xiao, Q.; Zhao, Y.; Wang, H.; et al. Evaporative Self-Assembly of Gold

https://dx.doi.org/10.1021/acsami.0c16315
ACS Appl. Mater. Interfaces 2020, 12, 54174−54180

Nanorods into Macroscopic 3D Plasmonic Superlattice Arrays. *Adv. Mater.* **2016**, *28* (13), 2511−2517.
(37) Yilmaz, M.; Babur, E.; Ozdemir, M.; Gieseking, R. L.; Dede, Y.; Tamer, U.; Schatz, G. C.; Facchetti, A.; Usta, H.; Demirel, G. Nanostructured Organic Semiconductor Films for Molecular Detection with Surface-Enhanced Raman Spectroscopy. *Nat. Mater.* **2017**, *16* (9), 918−924.
(38) Deegan, R. D.; Bakajin, O.; Dupont, T. F.; Huber, G.; Nagel, S. R.; Witten, T. A. Capillary Flow as the Cause of Ring Stains from Dried Liquid Drops. *Nature* **1997**, *389* (6653), 827−829.
(39) Ding, Q.; Wang, J.; Chen, X.; Liu, H.; Li, Q.; Wang, Y.; Yang, S. Quantitative and Sensitive SERS Platform with Analyte Enrichment and Filtration Function. *Nano Lett.* **2020**, *20* (10), 7304−7312.
(40) Talley, C. E.; Jackson, J. B.; Oubre, C.; Grady, N. K.; Hollars, C. W.; Lane, S. M.; Huser, T. R.; Nordlander, P.; Halas, N. J. Surface-Enhanced Raman Scattering from Individual Au Nanoparticles and Nanoparticle Dimer Substrates. *Nano Lett.* **2005**, *5* (8), 1569−1574.
(41) Liu, D.; Fang, L.; Zhou, F.; Li, H.; Zhang, T.; Li, C.; Cai, W.; Deng, Z.; Li, L.; Li, Y. Ultrasensitive and Stable Au Dimer-Based Colorimetric Sensors Using the Dynamically Tunable Gap-Dependent Plasmonic Coupling Optical Properties. *Adv. Funct. Mater.* **2018**, *28* (18), 1707392.
(42) Hao, Q.; Huang, H.; Fan, X.; Hou, X.; Yin, Y.; Li, W.; Si, L.; Nan, H.; Wang, H.; Mei, Y.; Qiu, T.; Chu, P. K. Facile Design of Ultra-Thin Anodic Aluminum Oxide Membranes for the Fabrication of Plasmonic Nanoarrays. *Nanotechnology* **2017**, *28* (10), 105301.
(43) Hao, Q.; Pang, J.; Zhang, Y.; Wang, J.; Ma, L.; Schmidt, O. G. Boosting the Photoluminescence of Monolayer MoS_2 on High-Density Nanodimer Arrays with Sub-10 Nm Gap. *Adv. Opt. Mater.* **2018**, *6* (2), 1700984.
(44) Hildebrandt, P.; Stockburger, M. Surface-Enhanced Resonance Raman Spectroscopy of Rhodamine 6G Adsorbed on Colloidal Silver. *J. Phys. Chem.* **1984**, *88* (24), 5935−5944.
(45) Otto, A.; Bruckbauer, A.; Chen, Y. X. On the Chloride Activation in SERS and Single Molecule SERS. *J. Mol. Struct.* **2003**, *661*, 501−514.
(46) An, J.; Tang, B.; Zheng, X.; Zhou, J.; Dong, F.; Xu, S.; Wang, Y.; Zhao, B.; Xu, W. Sculpturing Effect of Chloride Ions in Shape Transformation from Triangular to Discal Silver Nanoplates. *J. Phys. Chem. C* **2008**, *112* (39), 15176−15182.
(47) Zhao, L. B.; Chen, J. L.; Zhang, M.; Wu, D. Y.; Tian, Z. Q. Theoretical Study on Electroreduction of P-Nitrothiophenol on Silver and Gold Electrode Surfaces. *J. Phys. Chem. C* **2015**, *119* (9), 4949−4958.
(48) Xie, W.; Schlücker, S. Hot Electron-Induced Reduction of Small Molecules on Photorecycling Metal Surfaces. *Nat. Commun.* **2015**, *6* (1), 7570.
(49) Schmidt, M. S.; Hübner, J.; Boisen, A. Large Area Fabrication of Leaning Silicon Nanopillars for Surface Enhanced Raman Spectroscopy. *Adv. Mater.* **2012**, *24* (10), OP11−OP18.
(50) Huang, J. A.; Zhao, Y.; Zhu, X.; Zhang, W. Averaging Effect on Improving Signal Reproducibility of Gap-Based and Gap-Free SERS Substrates Based on Ordered Si Nanowire Arrays. *RSC Adv.* **2017**, *7* (9), 5297−5305.

https://dx.doi.org/10.1021/acsami.0c16315
ACS Appl. Mater. Interfaces 2020, 12, 54174−54180

Supporting information

Flexible Surface-Enhanced Raman Scattering Chip: A Universal Platform for Real-Time Interfacial Molecular Analysis with Femtomolar Sensitivity

Qi Hao[1,2,3‡], Mingze Li[1, ‡], Jiawei Wang[3,4], Xingce Fan[1,3], Jie Jiang[1], Xiaoxia Wang[3], Minshen Zhu[3], Teng Qiu[1,], Libo Ma[3], Paul K. Chu[5,6,7] and Oliver G. Schmidt[3,8]*

[1]School of Physics, Southeast University, Nanjing 211189, P. R. China

[2] Quantum Information Research Center, Southeast University, Nanjing 211189, P. R. China

[3]Institute for Integrative Nanosciences, Leibniz IFW Dresden, Helmholtzstraße 20, 01069, Germany

[4]Department of Electronic and Information Engineering, Harbin Institute of Technology (Shenzhen), Shenzhen 518055, China

[5]Department of Materials Science and Engineering, City University of Hong Kong, Hong Kong 999077, P. R. China.

[6]Department of Physics, City University of Hong Kong, Hong Kong 999077, P. R. China.

[7]Department of Biomedical Engineering, City University of Hong Kong, Hong Kong 999077, P. R. China.

[8]Material Systems for Nanoelectronics, Technische Universität Chemnitz, 09111, Germany

‡ These authors contributed equally.

*E-mail:tqiu@seu.edu.cn (T. Q.)

Fabrication of plasmonic nanoarrays using ultra-thin anodic aluminum oxide (AAO) membranes.

The plasmonic particle/dimer arrays are fabricated on silicon or quartz substrates by using anodic aluminum oxide (AAO) membranes in shadow evaporation. The AAO membranes are fabricated on aluminum foils by anodization method[1]. The AAO membranes are composed of a closely packed array of hexagonal cells with a cylindrical central pore extending down to the bottom (Figure S1). The AAO is designed with a tunable pore diameter from 20 nm to 95 nm with a controllable film thickness from 100 nm to several micros.

In order to get the porous nanomasks, the AAO membranes are peeled off from the aluminum foil in a replacement reaction where aluminum reacts with copper chloride. In our experiments, ultra-thin AAO membranes with a film thickness of less than 200 nm are required to insure good adhesion between the AAO nanomasks and substrates for subsequently shadow deposition. The ultra-thin AAO membranes are easy to fold or break into pieces because large amounts of gas and copper ash are generated during the vigorous reaction. In order to solve this problem, several tricks are adopted in the experiments: 1) A polymethyl methacrylate (PMMA) polymer layer is spin-coated on AAO/Al surface before the reaction. 2) Afterwards, a thick copper paper is placed on the sample surface and taped at the edges to prevent the entry of copper ash. 3) The protected sample is reversely fixed at the bottom of the container against bubbles generated during the reaction. 4) The generated copper ash is continuously cleaned by a dropper before the ash aggregates into tough bulk material on sample surface. 5) The concentration of copper chloride solution is 120 g/L based on the size of aluminum foil. A high concentration may result in sample broken while a low concentration may lead to the formation of CuCl deposits which is hard to clean.

The obtained PMMA/AAO membrane floats on solution. The film thickness and pore width of AAO could be further modulated by adjusting the phosphoric etching procedures[2]. The membranes are immersed in acetone to dissolve the polymer layer and transferred onto silicon or quartz substrates as nanomasks by Van der Waals force. In order to improve the adhesion between AAO masks and substrates, the silicon/quartz substrates are cleaned by NH_4OH/H_2O_2 solution at 75 °C to improve the hydrophilicity, which is crucial to the uniformity of the plasmonic nanoarray. Another tip for good uniformity is to make sure that the AAO membranes are transferred bottom up on the substrates with protuberance structures against the substrate. (Figure S1). Otherwise the membranes may fluctuate and fold on the substrate.

The prepared samples are used to produce particle/dimer nanoarrays by E-beam evaporation. The dimer arrays are fabricated with a specific deposition angle based on the length-width aspect ratio of AAO pores. After evaporation, the AAO masks are removed by a tape and the

patterned nanoarrays are obtained. The particle array instead of a dimer array is presented in Figure S1 because the gaps between dimers can be hardly distinguished in the 45° SEM images.

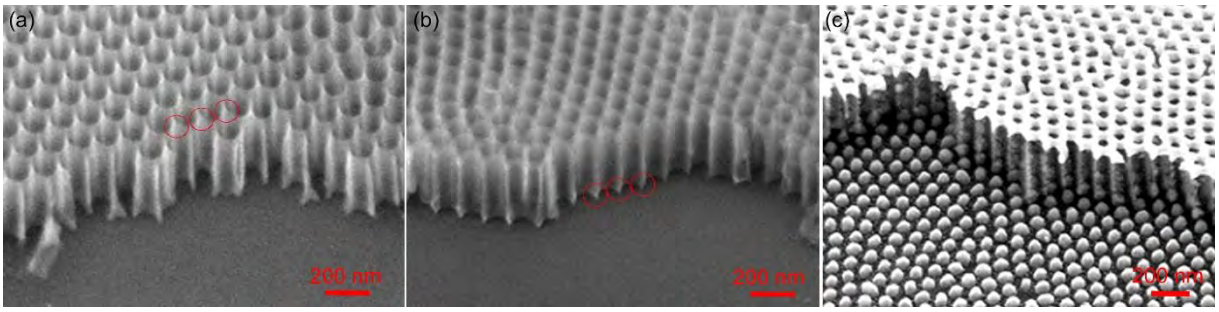

Figure S1. (a,b) Scanning electron microscope (SEM) images of ultra-thin AAO membranes placed face up (a) and bottom up (b) on silicon wafer substrates. The protuberances of AAO are marked with red circles. (c) An SEM image of a nanoparticle array fabricated by using an ultra-thin AAO membrane with E-beam evaporation.

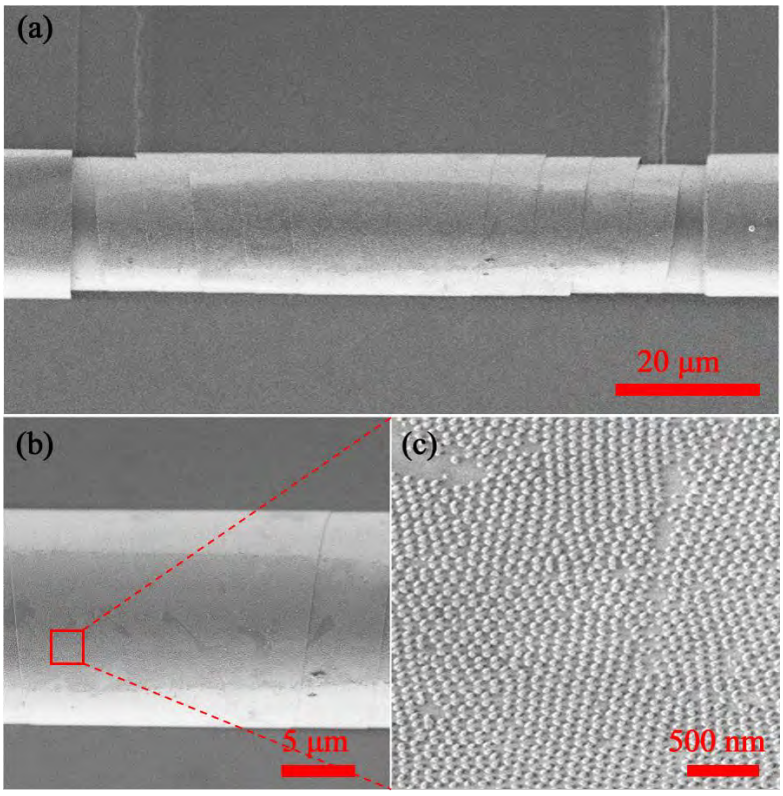

Figure S2. (a-c) SEM images of a microtube with plasmonc dimer patterns on top.

A proof of concept experiment is performed in demonstrating the good adhesion between the flexible SERS chip and substrates. A ridge microtube with winkles (a) is fabricated on wafer by rolled-up technique[3–5]. The SERS chip is transferred onto the microtube and immersed in acetone to dissolve the polymer. The SEM images show that the dimer particles are preserved on the tube with good patterns, suggesting a close contact between the particles and substrate even with irregular surfaces.

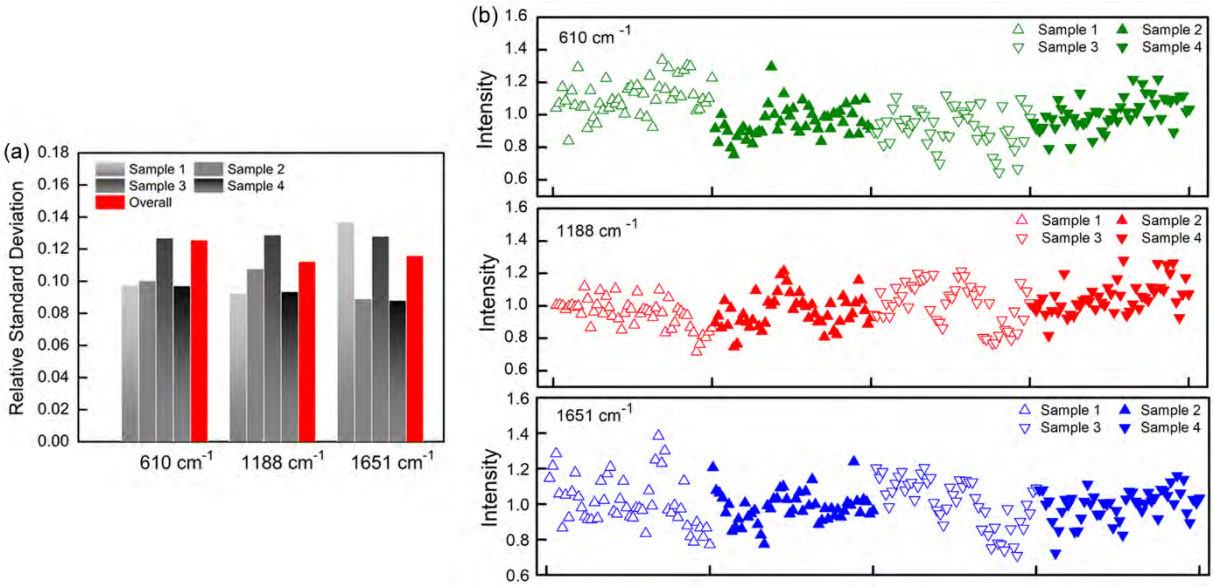

Figure S3. (a) Relative standard deviation (RSD) of the integrated intensity at 610, 1188 and 1651 cm^{-1} bands of R6G in liquid-state SERS measurements. The results are calculated by measuring 200 points from 4 samples fabricated under the same experimental conditions. (b) Integrated Raman intensity at 610, 1188 and 1651 cm^{-1} bands from the 200 points.

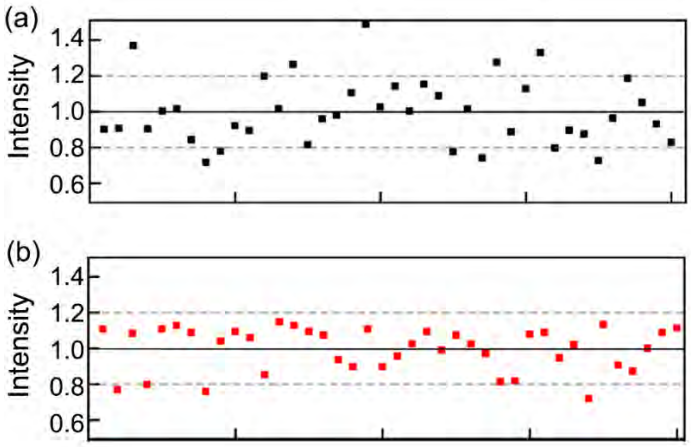

Figure S4. Dispersion of Raman intensity in solid-state measurement over a 1 cm^2 (a) and 10 um^2 area (b). The data are collected by analyzing the integrated Raman intensity of R6G at 1651 cm^{-1} from random sites. The two samples are prepared by using a half of one AAO nanomask to ensure identical nanoarrays are fabricated. It is observed the signal homogeneity is good over a limited area while degrades when the detection area is enlarged to the whole sample. The heterogeneity is not observed in liquid-state SERS, suggesting it arises from the preparation procedures in solid-state measurement.

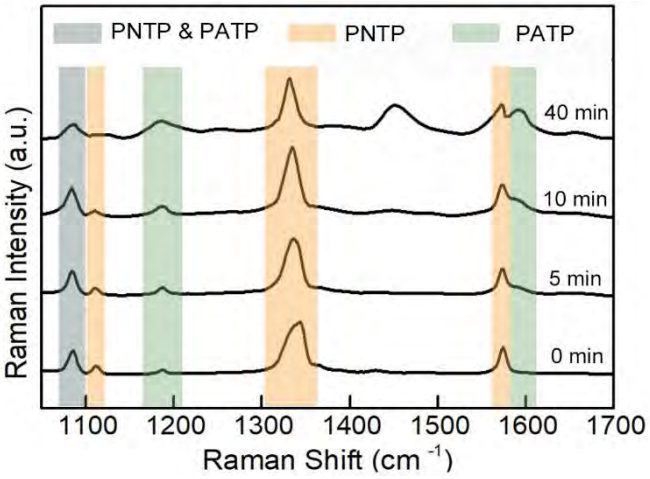

Figure S5. SERS dynamics of the reduction from *p*-nitrothiophenol (PNTP) to *p*-aminothiophenol (PATP) in hydrogen chloride solution. Partial of the PNTP molecules are reduced to PATP in 40 mins and no obvious changes are observed with further irradiation. The efficiency degrades in hydrogen chloride compared with it in hydrogen bromide.

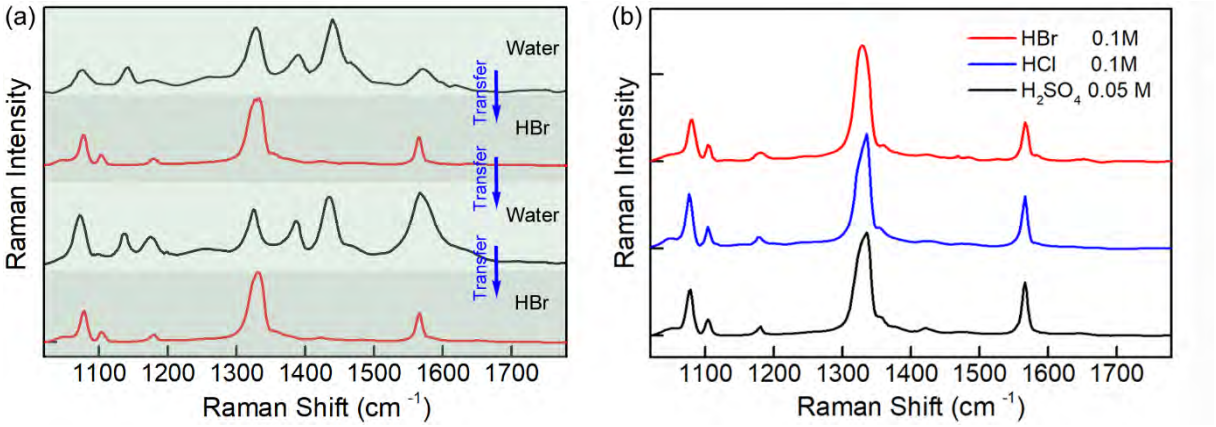

Figure S6. (a) Raman spectra of PNTP from the plasmonic chips under different environmental conditions. The chip is transferred between distilled water and 0.1 M HBr aqueous solution for several times. The characteristic peaks from PNTP are only observed in HBr solution while new surface specie *p,p'*-dimercaptoazobenzene (DMAB), an aromatic azo compound produced from the catalytic reaction on silver surface[6], is observed in water (or alkaline solution). (b) Raman spectra of PNTP from the chip in hydrobromic acid, hydrochloric acid and sulfuric acid solutions. The results suggest PNTP are stable in an acidic environment.

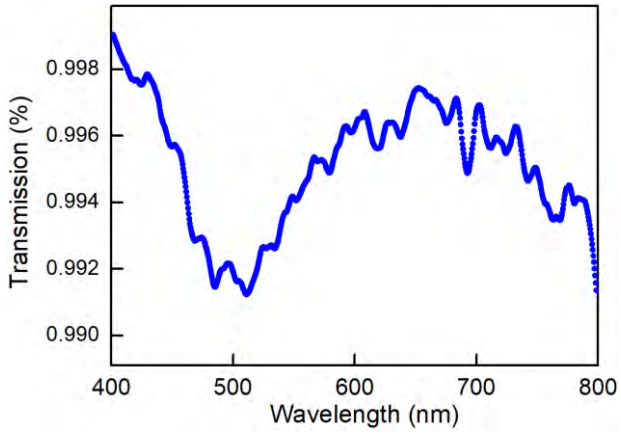

Figure S7. Transmission spectrum of a PMMA layer spin-coated on quartz glass. The PMMA polymer exhibits ultra-high transparency in the visible range.

REFERENCE

(1) Hao, Q.; Huang, H.; Fan, X.; Hou, X.; Yin, Y.; Li, W.; Si, L.; Nan, H.; Wang, H.; Mei, Y.; Qiu, T.; Chu, P. K. Facile Design of Ultra-Thin Anodic Aluminum Oxide Membranes for the Fabrication of Plasmonic Nanoarrays. *Nanotechnology* **2017**, *28* (10), 105301.

(2) Hao, Q.; Pang, J.; Zhang, Y.; Wang, J.; Ma, L.; Schmidt, O. G. Boosting the Photoluminescence of Monolayer MoS2 on High-Density Nanodimer Arrays with Sub-10 Nm Gap. *Advanced Optical Materials* **2018**, *6* (2), 1700984.

(3) Schmidt, O. G.; Eberl, K. Thin Solid Films Roll up into Nanotubes. *Nature* **2001**, *410* (6825), 168–168.

(4) Ma, L.; Li, S.; Quiñones, V. A. B.; Yang, L.; Xi, W.; Jorgensen, M.; Baunack, S.; Mei, Y.; Kiravittaya, S.; Schmidt, O. G. Dynamic Molecular Processes Detected by Microtubular Opto-Chemical Sensors Self-Assembled from Prestrained Nanomembranes. *Advanced Materials* **2013**, *25* (16), 2357–2361.

(5) Wang, J.; Yin, Y.; Hao, Q.; Yang, Y.-D.; Valligatla, S.; Saei Ghareh Naz, E.; Li, Y.; Saggau, C. N.; Ma, L.; Schmidt, O. G. Curved Nanomembrane-Based Concentric Ring Cavities for Supermode Hybridization. *Nano Letters* **2018**, *18* (11), 7261–7267.

(6) Wu, D.-Y.; Liu, X.-M.; Huang, Y.-F.; Ren, B.; Xu, X.; Tian, Z.-Q. Surface Catalytic Coupling Reaction of P-Mercaptoaniline Linking to Silver Nanostructures Responsible for Abnormal SERS Enhancement: A DFT Study. *The Journal of Physical Chemistry C* **2009**, *113* (42), 18212–18222.